JOURNAL OF COMPUTATIONAL PHYSICS **44**, 104–133 (1981)

Strong Ion Ring Equilibria Formed by Injection and Intrinsic Stochasticity of Orbits

ALEX FRIEDMAN*

Electronics Research Laboratory, University of California, Berkeley, California 94720

JACQUES DENAVIT

Department of Mechanical Engineering, Northwerstern University, Evanston, Illinois 60201

AND

R. N. SUDAN

Laboratory of Plasma Studies, Cornell University, Ithaca, New York 14853

An improved means of generating high-beta equilibria by injection in magnetostatic simulations of strong ion rings is described. The existence of stochastic orbits in these equilibria is demonstrated. For nonlinear axisymmetric two-dimensional simulations with all three velocity components included, the principal manifestation of such orbits is an eventual violation of left–right mirror symmetry in cases where such symmetry would normally be expected. This effet is due to the exponential divergence of "neighboring" mirror image trajectories. Linearized simulations, in effect, compute the first order separation of orbits which are displaced from each other by an infinitesimal vector for all time. When a linearized code is applied to a problem involving stochastic orbits, the single-particle growth can be faster than that associated with the collective modes of interest, rendering the simulation invalid. This limits the class of problems to which straightforward linearized simulation is applicable. Related difficulties in nonlinear codes using certain "quiet-start" techniques involving loading of particles on axisymmetric rings can be anticipated. These effects should also be evident in simulations of field-reversed mirror systems, ordinary mirror machines, and other devices.

I. INTRODUCTION

The term "stochastic" is applied to orbits which, loosely speaking, sweep out a nonzero volume of the appropriate phase space (the terms "chaotic" and "ergodic" also have been used by some authors to describe such orbits). Nonstochastic orbits are constrained by an additional constant of the motion to lie on a lower-dimensional

* Present address: Lawrence Livermore National Laboratory, Livermore, CA 94550.

0021-9991/81/110104–30$02.00/0

surface in this space, and so cannot sweep out a finite volume. Thick ion rings, with aspect ratios of order unity, have been found to include a fraction of stochastic single-particle orbits for moderate values of the field reversal parameter [1]. Some field reversed mirror plasmas may also entail stochastic orbits [1, 2]. These configurations are in contrast with infinitesimally thin "bicycle-tire" rings for which the poloidal angular momentum provides a constant of the motion for all particles, with axially-infinite layers for which the axial momentum is conserved, and with those mirror plasmas in which the magnetic moment is an adiabatic invariant. Furthermore, finite-aspect-ratio bicycle-tire rings and noninfinite long layer equilibria, and even certain model thick ion ring equilibria [3, 4], may also contain no stochastic orbits.

Excellent reviews of orbital stochasticity theory and related issues are available in the published literature, and the reader is referred to (in particular) Refs. [24, 5]. Here we briefly mention a few aspects of the theory which are of direct relevance, and attemt to clarify some terminology; the latter is by no means standardized.

The stochasticity of orbits in a system such as the one we are considering is termed "intrinsic" because it is inherent in the particle motion in a static field—no collisional effects are involved. While motion in the full phase space is deterministic, the intersections of a trajectory with a slice of the phase space appear to be random.

One aspect of stochastic-orbit equilibria is of particular concern to simulation models in general and linearized simulations in particular. This is their property of "local" or structural" instability, whereby neighboring trajectories diverge from each other exponentially with time, at least when viewed on a timescale long compared with the system's characteristic timescale (for ion rings this is the self field betatron timescale). The rate of separation of neighboring orbits is alternately termed the "Kolmogorov entropy" (although it has the dimensions of a frequency) [5] or the Liapunov exponent [6]. When orbits are stochastic, the Kolmogorov entropy is positive. Strictly speaking, stochasticity (in the sense that a third invariant is absent) is always present when local instability (in the sense of exponentially diverging orbits) is present, but the converse is not rigorously true, though it is generally true in practice [7–9]. The term "ergodicity," though often used synonymously with "stochasticity," is more usually taken to refer to an equivalence of time and ensemble averages or an arbitrarily close approach of the trajectory to all points of the energy surface. The term "chaotic" (used as an adjective to describe trajectories) appears to us to be synonymous in the literature with either "stochastic" or "locally unstable"; it is generally used to describe the aperiodic motion that can arise even in simple mappings and dynamical systems [24]. In any event, it is the property of local instability which is of primary interest here, as this is what is measurable in the simulations. Also of interest is the stochastic nature of the unstable orbits as evident in their surface of section plots, described below. In this paper the term "stochastic" will generally be used in favor of "ergodic" or "chaotic"; it should be understood that the rapid divergence of neighboring orbits is implied, since in our simulations stochasticity and local instability have always appeared together.

The RINGHYBRID code [10] is a linearized hybrid code which assumes an

axisymmetric magnetostatic equilibrium. It models the evolution of linearized non-axisymmetric (3d) perturbations about this equilibrium. Using this code, we have observed two manifestations of orbital stochasticity. The first is evident in the zero order motion of particles in an ion ring, appearing as an eventual violation of mirror symmetry about the plane $z = L/2$, and is probably not of serious consequence. We confirm the existence of both stochastic and nonstochastic zero order orbits by means of surface of section plots. The second manifestation is a ragged exponential growth of the first-order separation of the displaced and undisplaced particles. Stochasticity is evident in the linearized motion because $\mathbf{B}^0$ is evaluated at the *perturbed* particle location; the perturbed orbit is always a "neighbor" of the unperturbed orbit, and so their separation can grow exponentially as they move in the equilibrium field. Since this growth can be rapid, it can easily mask the behavior of the collective modes which are the real objects of study in linearized simulation, thereby rendering the simulation invalid.

In Section II we describe the means by which equilibria are generated, and present a simple infinite-layer example. Section III describes an ion ring equilibrium, and the observation of stochastic orbit effects in the simulation of particle motion in this equilibrium. Section IV describes the effects of orbital stochasticity as manifested in the motion of the displacements between unperturbed and perturbed orbits in the linearized simulation. Section V summarizes this work, and presents our conclusions.

II. Generation of Equilibria

The modelling of axisymmetric high-beta systems, such as field reversed particle rings or mirror plasmas, via particle-in-cell simulation techniques often requires the generation of an appropriate equilibrium. Such a state can never be truly time-independent, since the equilibrium orbits do not constitute a laminar flow pattern, but rather entail chaotic particle motion. Since the number of particles used is finite, it follows that fluctuations in the fields will persist even if great care is used in initializing the equilibrium. Nonetheless, it is desirable to be able to attain as quiet an equilibrium as possible by minimizing fluctuations of the fields and of the macroscopic moments of the particle distribution. We present here a technique which has been found useful in this regard.

There are two ways by which high-beta equilibria have been created in particle codes. The first of these involves the implementation of an approximation to a Vlasov equilibrium, either known analytically [11], or obtained from another computer program [12, 13]. By appropriate integrals over the distribution function one obtains the density at each point in space and assigns particles to positions in the r–z plane accordingly. The velocity distribution at each point is then modeled by assigning velocities to the various particles in such a way that the distribution of velocities has approximately the same moments as the desired Vlasov distribution. Due to the finite cell size, time step, and number of particles used, some errors are introduced, but in

general equilibria formed by this method should be quiescent enough for most purposes. The main drawback of this method is the complexity of implementation; this is especially true for cases in which the equilibrium distribution is not expressible in closed form, or entails more than one nonignorable spatial coordinate, so that there is no unique inversion of the density distribution into the set of initial particle locations. Another drawback is the arbitrariness of the distribution function chosen; one chooses between (say) the rigid-rotor or double-delta-function forms on the basis of physical intuition.

A much simpler alternate method which is often employed involves the expedient of injecting pulses of particles at appropriate points in space over a period of time. This emulates the physical process of creating a plasma by neutral beam injection. We would then expect to observe non-equilibrium behavior of the injected particles. Coherent motions would persist indefinitely in the system; for example, in a ring-equilibrium of energetic particles whose orbits encircle the axis, we expect oscillations in the mean particle r-coordinate at approximately the cyclotron frequency, a so-called breathing motion of the ring. This is due to orbits of each elements of the ring being off-center. Similarly, we would expect oscillations in the minor dimensions of the ring due to coherent betatron motion of the particles—this effect would be expected to phase-mix away to a large degree, while the former would not. We thus seek a means for damping collective oscillations out of the system, while ensuring that currents and fields be consistent when equilibrium has been reached.

The model we consider assumes neutralization of currents in the r–z plane, and of all space charge. The azimuthal current is not neutralized. Thus, the vector potential is $\mathbf{A} = A_\theta \hat{\theta}$ and the fields are described by $\mathbf{B} = \nabla \times \mathbf{A}$ and $E_\theta = -\partial A_\theta / \partial t$. We obtain the vector potential from a modified Ampere's law:

$$\nabla \times \nabla \times A_\theta^s \hat{\theta} = (J_\theta - \sigma \, \partial A_\theta^s / \partial t) \, \hat{\theta},$$

where A_θ^s is the self-field component of A_θ and the transverse displacement current is neglected in the usual magnetostatic approximation. Here, σ is a constant which has been introduced to correspond to an effective (artificial) conductivity. Neglecting the source term, J_θ, this field equation has the form of a diffusion equation, and may be solved using a time-centered Crank–Nicholson finite difference representation, or by a simpler implicit backward difference, which is entirely adequate for the present purpose.

The inclusion of the new (σ) term brings about a dissipation of the energy associated with collective motions. While particle orbits in equilibrium do not lead to time-varying currents and fields, collective motion such as breathing leads to a time-varying vector potential. This causes azimuthal pseudo-currents $-\sigma \, \partial A_\theta^s / \partial t$ to flow in the system, peaked in those regions where the collective motion causes the most change in A_θ. By Lenz's law, the locations and temporal phases of these currents will be such as to bring about modifications to E_θ and $\mathbf{B}$ that will damp the undesirable oscillations. During the setup of an equilibrium, energy is dissipated; the amount lost

is given by the integral over all space and from the time of initialization until the present time of the Ohmic loss per unit volume and time, $\sigma(\partial A_\theta/\partial t)^2$, a quantity which can be monitored so that a check for overall energy conservation is still possible. This damping effect is similar to that of the azimuthal resistor wires used in the Astron device [14]. The purpose of these wires is to damp axial motion (and to a very slight degree, radial motion) of the energetic particles; this has been modeled in simulations of the Astron [15, 16], and of proton ring trapping experiments [17, 18]. The present scheme damps axial and radial motion, and does not concern itself with the quantitative evaluation of damping effects. Hence, the simple backward difference is adequate, while codes which model physical resistive effects should normally employ a more sophisticated numerical scheme. The self-magnetic field (hence beta) must be fairly large for this method to work; this can be seen by noting that in the zero-beta test-particle limit all forces on a particle arise from externally generated fields, and so no damping of collective oscilltion can arise from interparticle forces.

Appropriate choice of the constant σ is made by the observation that damping will be most effective if it is near-critical; that is, the time scale of the oscillations to be damped should be matched by an L/R time corresponding to a inductor with dimensions those of the high beta plasma system (gradient lengths) and conductivity σ. In actuality the value of σ need not be carefully chosen—almost any roughly reasonable value will work fairly well, and a trial-and-error procedure can be used to refine a poor initial guess.

As equilibrium is reached, the size of the resistive term diminishes, until it becomes entirely negligible. If collective oscillations of several different timescales need be damped, σ might be changed as time goes on; or, the damping might be eliminated altogether if perturbations will be applied to the equilibrium and a natural response of the particles is desired.

Presented in Fig. 1 are results obtained using an infinite-layer 1d2v (one spatial coordinate, two velocity coordinates) version of the zero-order (equilibrium) portion of the linearized hybrid code RINGHYBRID [10], which in the more general case models a 2d3v equilibrium, assuming azimuthal symmetry only. In this example we have assumed an infinitely long system, so that $\partial/\partial z = 0$, for simplicity. Other results using this code, and using RINGA, a fast 2d3v particle code [17, 18], confirm that the technique works well for finite length equilibria as well. In the run shown, a total of 600 super-protons were injected over 50 timesteps, at 12 evenly spaced injection radii between 10 and 24 cm. (the wall was at 24 cm.). The cyclotron period in the external field was 80 timesteps; including self-field effects (hoop stress and image currents) the mean gyration period was about 110 timesteps. The mean radial betatron period was somewhat shorter; usually the limit on the size of the timestep which may be taken is set by this betatron period, but in this case the timestep was smaller than necessary due to limitations set by the first-order part of the code, not relevant to this discussion. Enough particles were injected so that the self-magnetic field under the layer was 70% of the applied field. Other parameters for this run are: $\Delta r = 1$ cm., $\Delta t = 1$ ns., $v_{\text{injection}} = 0.76 \times 10^9$ cm/sec at $r = 12$ (varies proportional to r), and $B_{\text{ext}} = 8$ kG, so that $\omega_{ci}\Delta t = 0.07854 = 2\pi/80$. There were 3.9×10^{15}

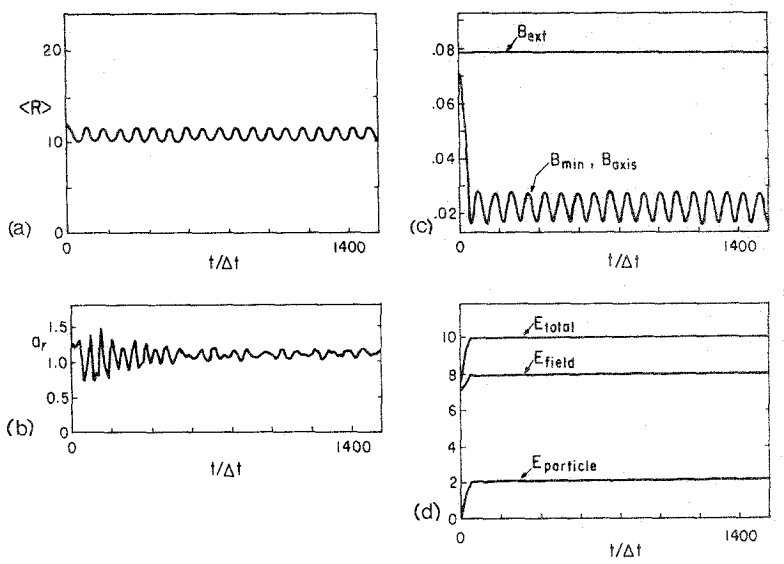

FIG. 1. Quantities as functions of timestep for infinite layer run without resistive damping: (a) Average radius. (b) Radial RMS halfwidth. (c) Magnetic field: external, on axis, and at point of maximum reversal (the last two are superposed here as no pseudo-currents flow between the layer and the axis). (d) Particle, field, and total energies. Note that the total injected particle energy in these units is 2.8; the difference is due to the fact that the first particles injected experience an E_θ due to injection of later particles.

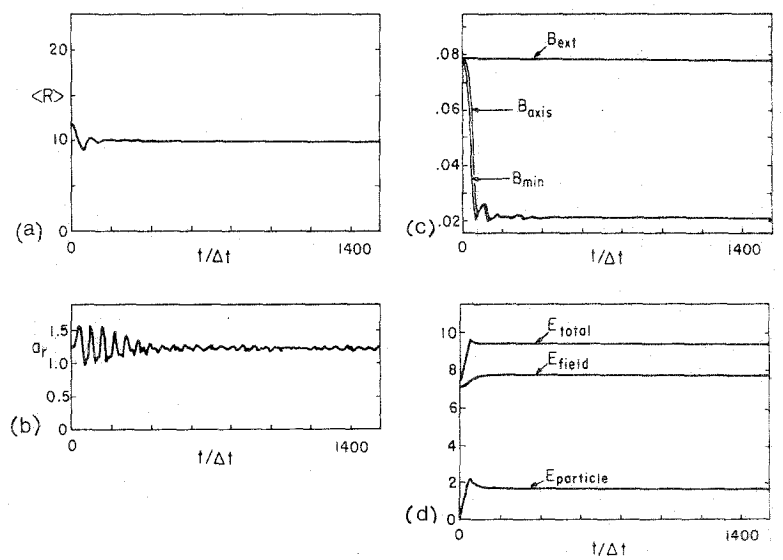

FIG. 2. The same quantities for a run identical to that of Fig. 1 except that σ was set to 8 mho/meter (1, in dimensionless units).

protons per unit axial length, and a typical ion density was 1.3×10^{13} cm^{-3}. Note the persistent collective motion, especially that of the major radius, in the figure.

Figure 2 shows results for a similar run wherein a damping term $\sigma = 8$ mho/meter (or, in "internal" dimensionless units, 1.0—see Ref. [10]) was added to the field solution. Here, the collective oscillations are seen to damp away. (Numbers appearing at the sides of the plots are in dimensionless units, included to facilitate comparisons between the two runs, while numbers along the lower edges of the plots indicate timesteps.) It should be noted that the parameters of this run were the first ever tried with this system; no fine-tuning of σ whatsoever was done. It is evident that inclusion of the resistive term greatly influences the motion, and that only the energy associated with collective ring motion is removed.

III. Stochasticity in the Zero Order Simulation

A. *Observation of Stochasticity; Loss of Symmetry*

The first manifestation of stochasticity is evident in the zero order particle orbits. Particles are injected over a number of timesteps to build up an approximate equilibrium possessing mirror symmetry about the plane $z = L/2$. That is, for each particle with phase-space location $(r_1, z_1, v_{r1}, v_{\theta 1}, v_{z1})$ there is another particle at $(r_2, z_2, ...) = (r_1, L - z_1, v_{r1}, v_{\theta 1}, -v_{z1})$. Self-consistent fields are calculated using the modified Ampere's law described in Section II, above. After allowing the equilibrium to "settle down" and any gross collective oscillations to phase mix out (for perhaps 500 timesteps), fields are "frozen" so that the linearized simulation employs time-invariant "equilibrium" fields. In contrast with the observed behavior of extremely thin bicycle-tire rings wherein left–right mirror symmetry obtains throughout the run, in the thicker rings studied mirror symmetry is seen to persist for a time on the order of 1000 timesteps, after which it is observed to break down for some of the particles. This can be interpreted as follows: the mirror image particles are in fact only mirror images to one part in (say) 10^{13}—roundoff errors in the computation guarantee that no exact mirror symmetry can obtain. Thus, except for the axial reflection about $L/2$, these two orbits can be considered to be "neighboring trajectories." These diverge exponentially in time (with noise superposed), and eventually the difference between the two orbits (i.e., $z_1 + z_2 - L$) has exponentiated from 10^{-13} to unity, and the orbits become visibly different.

A specific example is the run "JVA" (which was re-run as "JWA" with different diagnostics). For this run 2400 simulation particles were employed, the major radius was $r_0 = 15$ (cells), the wall was at $r_w = 24$, and the periodicity length L was 24. The radial and axial *rms* halfwidths were 2.0 and 2.8, respectively (due to finite particle size the effective halfwidths are somewhat larger). The external-field cyclotron period was 40.0 (timesteps), the mean gyration period being increased to 42 by self-field effects. A nominal betatron period, obtained by integrating over J_θ (as in Eq. 27 of Ref. [19]), was 52 timesteps, although axial and radial betatron periods differ greatly

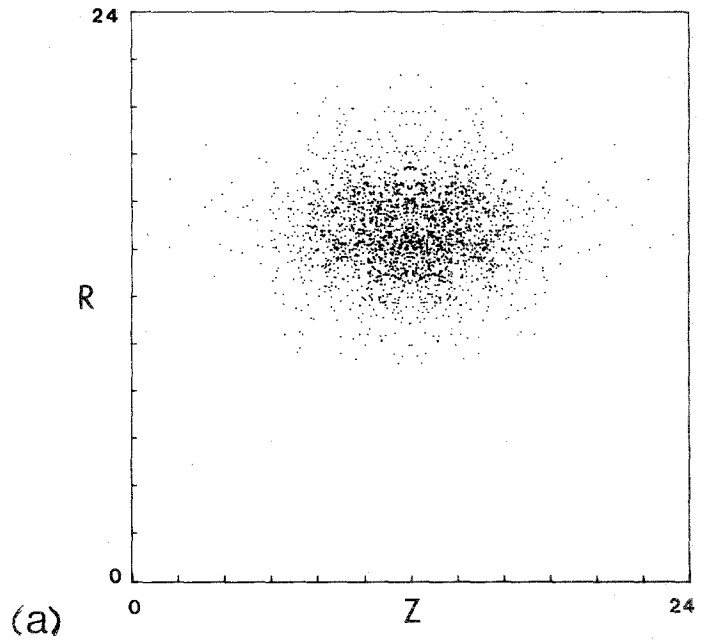

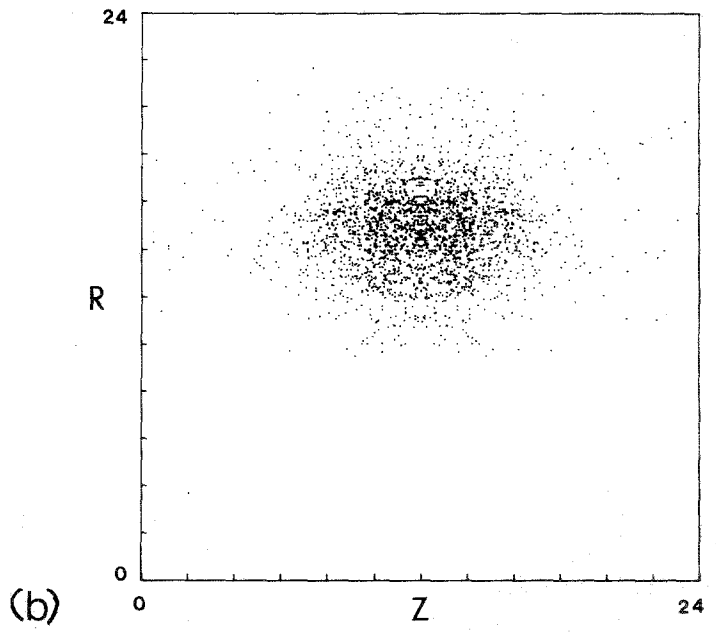

FIG. 3. (a) Particle locations in the r–z plane at timestep 500. Note the absence of asymmetry about $z = L/2$. (b) Particle locations in the r–z plane at timestep 2000. Asymmetry about $z = L/2$ is now evident.

for a ring of this geometry. The field reversal factor (ratio of self to external magnetic field magnitudes) was 18% on axis, and 25% immediately under the ring. For this run the absolute convergence criterion for the zero order field-solver was set to EPS $= 10^{-13}$, so that the initial symmetry was good to somewhat fewer than 13 digits, taking error propagation on the mesh into considertion (the magnitude of A_θ is of order unity in these simulations). The resistive relaxation term σ was used with a (dimensionless) value of 0.125, and zero order fields were "frozen" at timestep 450.

Snapshots of the ring at timesteps 500 and 2000 are presented in Figs. 3a and b, respectively. Asymmetries, especially in those particle orbits with large axial excursions, are evident in the plots at IT $= 2000$.

Figure 4 shows the orbits of a pair of particles which were initially mirror images of each other. For each particle r and z are plotted as functions of time. Mirror symmetry is seen to obtain until approximately timestep 1100, at which point the orbits become visibly different (much easier to see on a larger plot—on this one the orbits differ visibly only after another 100 timesteps or so). The straight vertical lines are the result of the periodic particle boundary condition being inforced when a particle passes through $z = 0$ or $z = L$. Note that this pair of particles was selected to illustrate the eventual breaking of mirror symmetry—not all pairs of particles would have shown this effect.

Using an interactive debugging routine, the quantity $z_1 + z_2 - L$ was printed out at every other timestep. From this printout the growth rate of the separation of the "neighboring" mirror image orbits could be calculated. The timestep at which each decade of separation was first reached was noted:

decade -11 was first reached at IT $=$	90
-10	230
-9	296
-8	332
-7	404
-6	616
-5	728
-4	764
-3	872
-2	956
-1	1068.

We thus find a decade time of roughly $(1068 - 90)/10 \approx 100$ timesteps. The corresponding growth rate is comparable to the betatron frequency. Plots of this quantity for a similar run are shown in Fig. 7, discussed below.

To further verify that we are not simply observing a code "bug," runs were carried out using other values of the zero order fieldsolver convergence criterion, EPS. Larger values of EPS lead to larger ripples in the field and hence larger initial perturbations to particle orbits. The stochastic growth *rates* are unchanged by varying EPS, as the field itself is the same to eight or nine digits at worst. Run "JYA" used EPS $= 10^{-11}$;

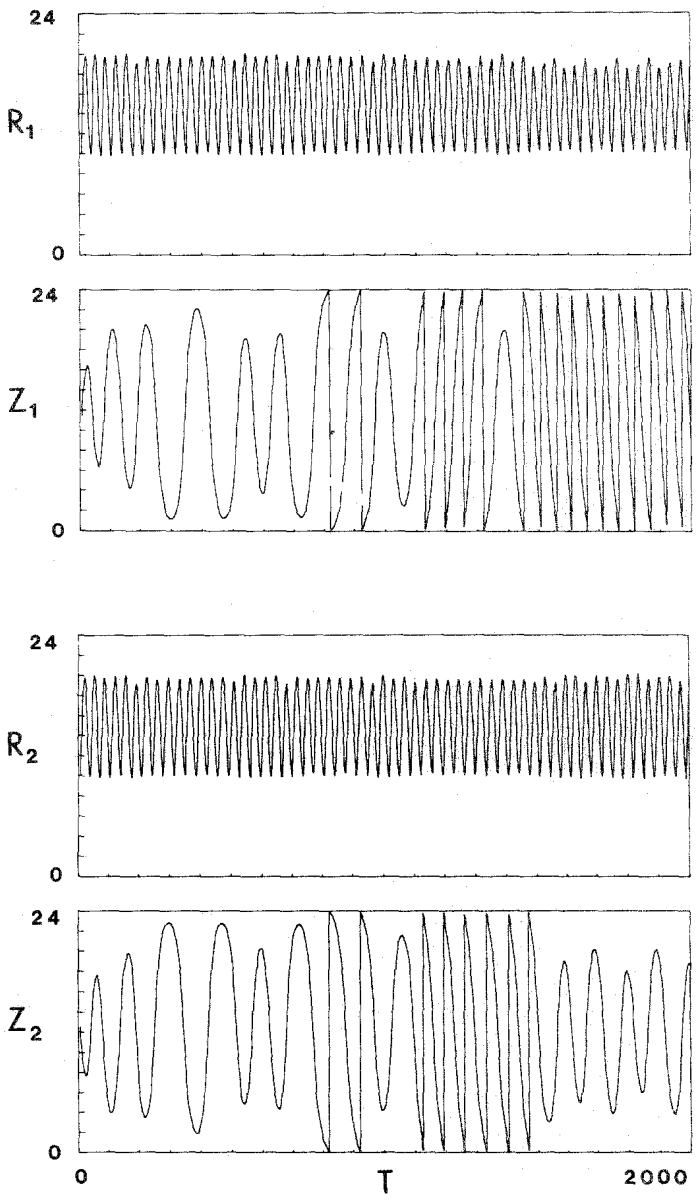

FIG. 4. The orbits of a pair of particles which were initially a mirror image pair, selected from run JWA with EPS = 10^{-13}. The histories of r and z as functions of time are shown. Mirror symmetry about $Z = L/2$ is evident until approximately timestep 1100.

for this run a difference was visible (on a large copy of Fig. 5) at about IT = 1075. This is not much earlier than in JWA, but recall that the growth is noisy and that absolute precision of the computer is about 14 digits, so that JWA's value of EPS probably cannot give much better accuracy than the less stringent value used in JYA. To see the effect more clearly, another run, "KAA," was made using EPS = 10^{-9} (see Fig. 6). For this run differences between the mirror image particles are visible at roughly IT = 825. This is about 250 timesteps earlier than in run JYA; since this run had an initial perturbation roughly 100 times as large as JYA, it would be expected to need two decades, or on the order of 200 timesteps, less growth for the sepration to be visible (consistent with the value of 250 observed). Note that the field solver does not enforce exact left–right symmetry, and so the fields themselves exhibit a small amount of asymmetry which is larger for larger EPS. As stated above, the rate of orbit separation does not change with EPS, and so we conclude that the additional left–right field asymmetry does not significantly affect the orbital asymmetry except for starting it at a higher level initially. Other simulations carried out enforcing field symmetry revealed similar stochastic behavior.

Even though the orbits diverge greatly, energy conservation for both is excellent since only "rotations" of the velocity in the magnetic field are performed. Conservation of canonical angular momentum P_θ is not trivially guarantted by this algorithm, but is always valid to within a few percent even in the worst cases. Field quantities are functions of r and z alone, and are thus perfectly axisymmetric, but since the field **B** and not the vector potential A_θ is employed in the acceleration, the canonical angular momentum calculated as a diagnostic can vary with time. Deviations are not systematic, and become smaller as the cell size and timestep are reduced. Stochastic effects persist when this is done, a further assurance that they are not a result of numerical imperfections.

B. *Stochasticity and Confinement*

The zero order effect eventually leads to a lack of symmetry of the ring; this is partly due to the small number of particles leading to fluctuations that only seemingly violate axial momentum conservation (consider a single particle in a mirror field—its axial momentum is not conserved). The effect is magnified by the periodic particle boundary condition; if one of the ex-mirror image pair of particles reaches the boundary at $z = 0$ or L, and the other does not, the center of mass of the ring shifts to one side or the other.

In addition, a particle may leave the ring (by entering the "loss cone") even after it has exhibited a large number of betatron oscillations whithin the confines of the ring; such a particle must be considered an "unconfined particle." An example is shown below wherein one particle was unconfined (first reached $z = 0$ or L) at timestep 2600, while its "mirror image" was confined until timestep 8400. The equilibrium fields of necessity include contributions from this class of particles. Lovelace *et al.* have shown that exponential rigid rotor equilibria, for example, contain a class of unconfined orbits [20, 21].

There appears to be a correlation between whether or not a particle's orbit is

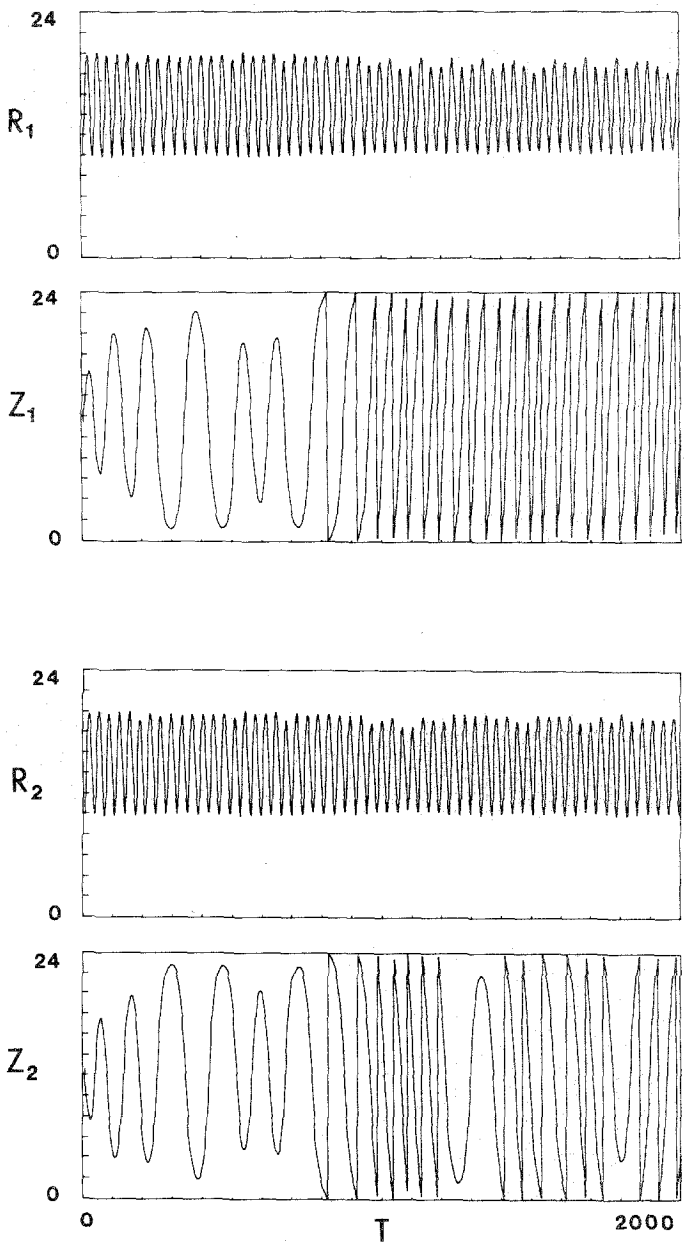

FIG. 5. The same quantities from run JYA with EPS = 10^{-11}. Symmetry holds until approximately timestep 1075.

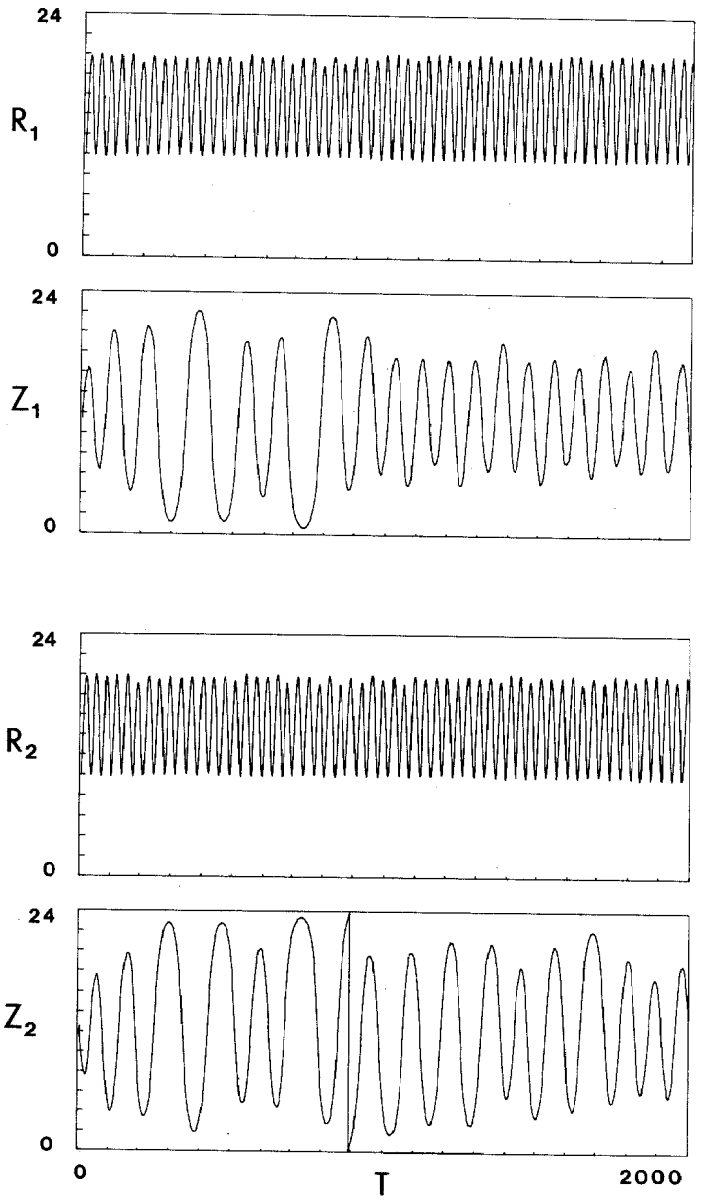

FIG. 6. The same quantities from run KAA with EPS $= 10^{-9}$. Symmetry holds until approximately timestep 825.

unconfined and whether or not it is stochastic (as expected, since both are associated with high energy), but it is not one-to-one. That is, some apparently confined particles show stochastic motion–one cannot be sure they are in fact confined without making an infinitely long run, at least with the usual scheme of injection wherein random velocities are added to the injected particles (in a mirror-symmetric manner). Most recently, a run (KKA) was made wherein no random velocities were added. In this run each group of injected particles chould only self-pinch together, and lose energy due to the inductive electric field when succeeding groups of particles were injected. Thus, all particles were necessarily confined (this was observed to be the case); nonetheless, the stochasticity—induced asymmetry was present in this run. Note that this method of injection gave an equilibrium which was not at all like a rigid rotor in that the angular velocity showed high shear.

On energetic grounds one expects a different relationship between confinement and stochasticity depending upon whether the particle orbit encircles the axis (ion ring case) or does not (small-orbit mirror plasma, most particles). In the former, the level surfaces of the effective potential are closed, so that particles of small enough energy must be absolutely confined, while in the latter, the surfaces extend to infinity and confinement normally depends upon the particle pitch angle [22]. Jumps in the adiabatic invariant μ associated with stochasticity effectively enlarge the loss cone so that all stochastic orbits which do not encircle the axis are unconfined and should be excluded from the equilibrium [2]. However, for the ion-ring case (and for large orbit field reversed mirrors as well) our experience suggests that an appreciable number of [redacted] for an arbitrarily long time interval; see Section E below for an example.

We note in passing that in connection with the adiabatic invariant μ the non-stochastic regime is often referred to as "superadiabatic" [2]. In this regime jumps in μ with each traverse of the system are not independent of each other, but are correlated in phase; successive μ values lie on a bounded curve which is a periodic function of time, and on a surface of section plot a superadiabatic orbit traces out a closed curve.

C. *System Length and "Unfrozen" Fields*

Runs were made using a larger number of cells axially (a larger vacuum region on each side of the ring, and a longer periodicity length—the cell size was kept constant). Run "JZA" used 48 cells in z, while "KBA" used 96 cells. In general, we observed that the longer the periodicity length, the longer it took for the (same) two test particles to show asymmetry. Note that asymmetry showed up in the latter run even though the test pair did not reach the axial boundary during the run, but took nearly to timestep 2000 to do so, in contrast with the shorter systems described above wherein asymmetry was visible after about 1000 steps. Presumably this change in the rate of growth of asymetry occurs because the shape of the effective potential well is different for the various system lengths, both due to the boundary condition on the fieldsolver being imposed at different places and due to the fact that in the axially

short runs the particle periodicity condition was enforced more often during the setting up of the equilibrium fields. We do not anticipate that making the system even longer would reduce the stochastic behavior to any great degree, since the 96-cell system is already much longer than the ring. However, we have not verified this conjecture.

For the axially long systems, the axial halfwidth of the ring was observed to increase at long times both more rapidly and to a larger value than in the shorter systems (with similar rings but different "tanks"). Presumably this is due to the fact that when particles find their way into the "loss cone" they have a larger distance to travel before reentering the ring region one axial period later, and so the halfwidth can grow appreciably. The growth in axial length is associated with unconfined (high energy) particles, and so tends to be present when stochastic orbits are present.

The breaking of mirror symmetry, and the axial halfwidth growth as well, were present even in a run wherein the zero order fields were never "frozen"; in fact the

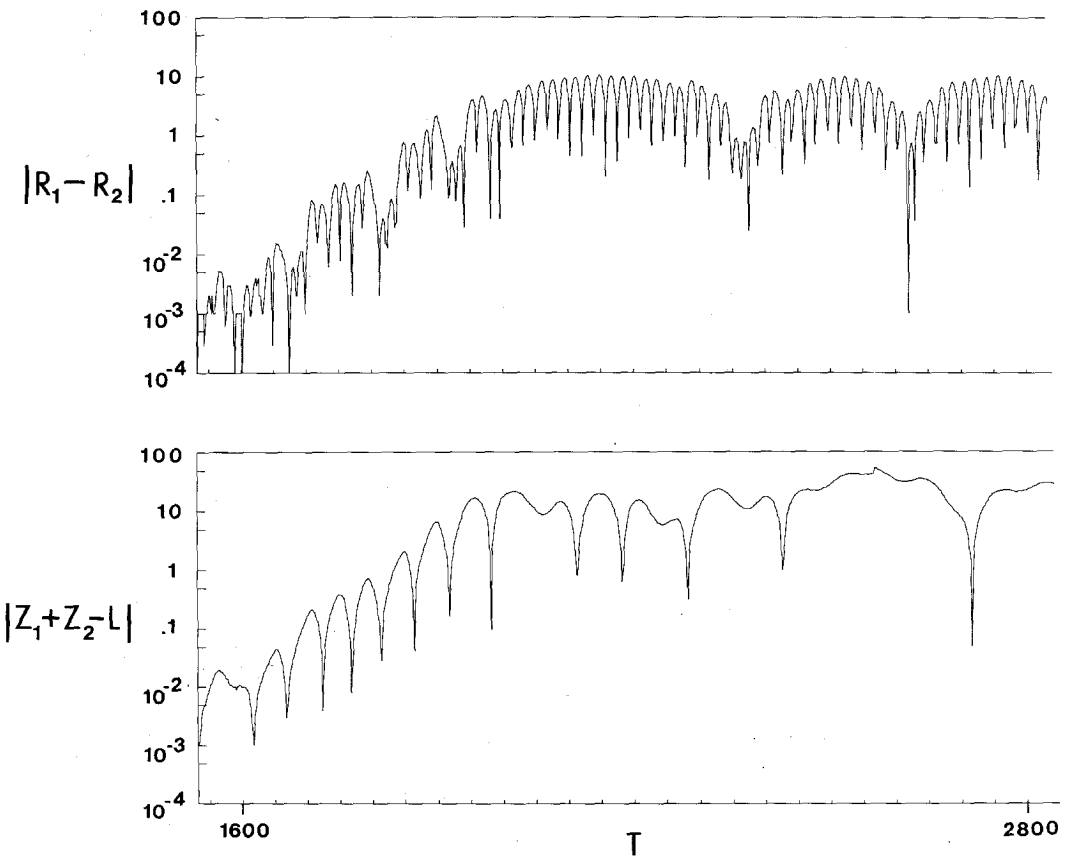

FIG. 7. Plot of $|r_1 - r_2|$ and $|z_1 + z_2 - L|$ as functions of time for a run with $L = 96$. The maxima of these quantities are seen to be of order the system size.

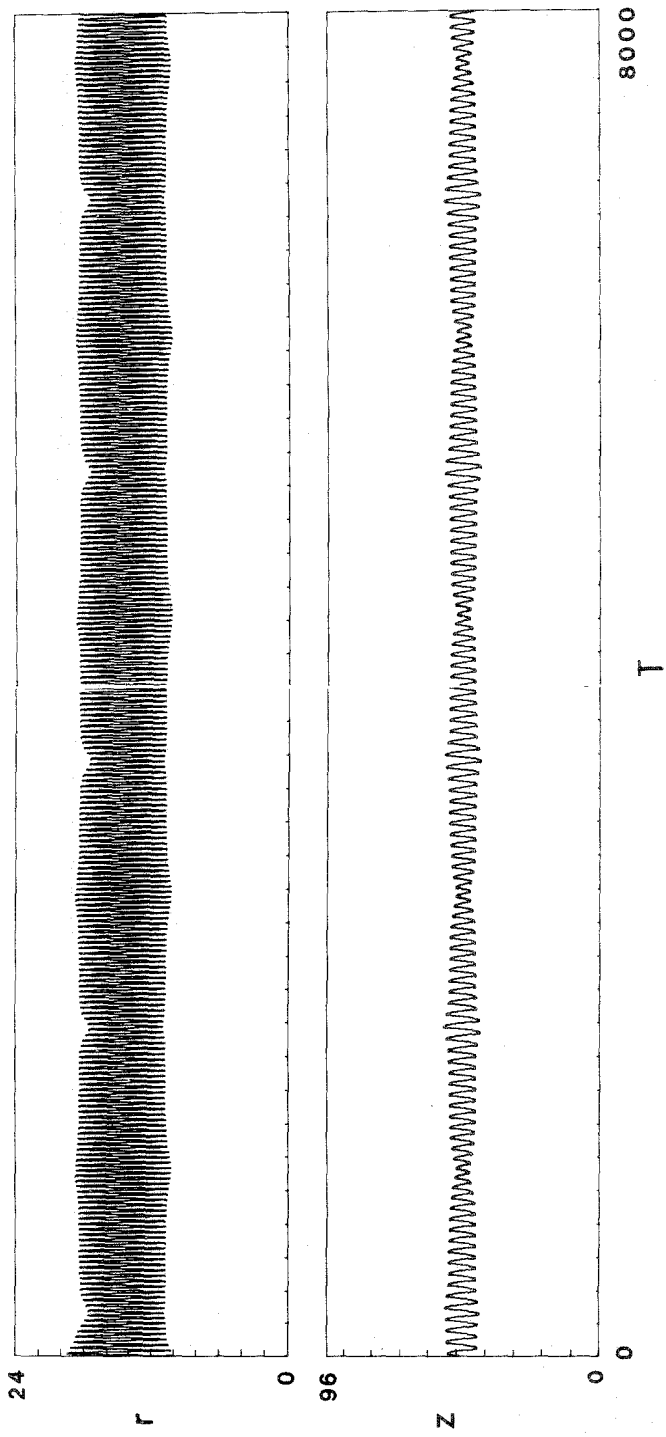

FIG. 8. R and z histories for a nonstochastic particle selected from a run with $L = 96$, over a period of 8000 timesteps.

halfwidth growth was somewhat *more* pronounced in this case. We conclude that keeping fields "unfrozen" does not reduce the effects of stochastic orbits.

D. *Implications of Loss of Symmetry*

We believe this loss of symmetry has not been noted previously in simulations of field-reversed ion rings and mirror plasmas, although it may have been present in runs of SUPERLAYER [15, 16] or RINGA [17, 18]. Normally, small deviations from symmetry (in runs where symmetry would be expected) are not measured in such simulations, and in a nonlinear 2D3V code these are the only quantities which grow exponentially. Also, "saturation" of this effect must set in when the amplitude becomes comparable to the system size, or perhaps more properly to a smaller "island width" of the stochastic region in the $r-z$ projection of phase space [2]. Figure 7 shows the quantities $|r_1 - r_2|$ and $|z_1 + z_2 - L|$ plotted as functions of time

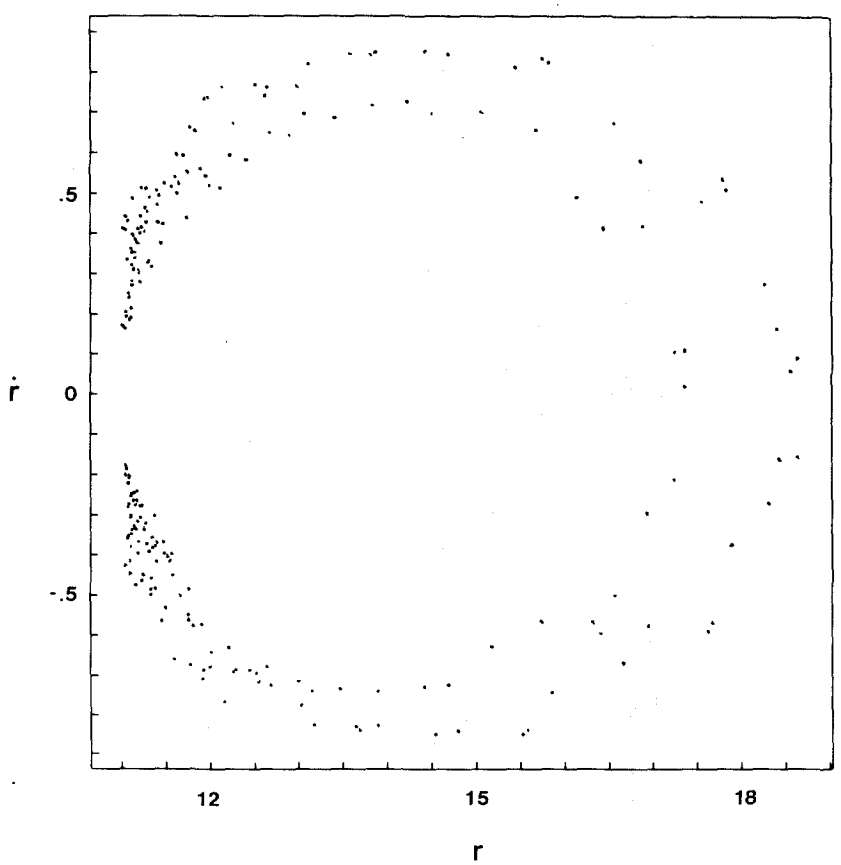

FIG. 9. A surface of section plot for the particle of Fig. 8, as described in the text. Diagnostics were performed every other timestep, and linear interpolation between these points was used. Note that points fall on a crescent but do not fill the area enclosed by the crescent.

for a run with $L = 96$. The last three decades of exponential growth, and the "saturated" state, can be seen. Here "saturation" appears to occur when the separation of the orbits is of order the system size.

The loss of symmetry to zero order probably is not of great fundamental consequence by itself. One could simulate only the region $Z > L/2$ for example, enforcing the mirror symmetry for all time, if one were only interested in the zero order ring behavior.

E. *Surfaces of Section and Stochasticity*

To confirm that we are in fact observing both nonstochastic and stochastic orbits, surface of section plots were generated. These show the prticular values taken by r and $\dot{r}$ of each particle as the particle passes through $z = L/2$. Such plots, and variations using other variables, have been employed previously to show orbital stochasticity [1]. They depict a "slice" of the phase space through which the particle

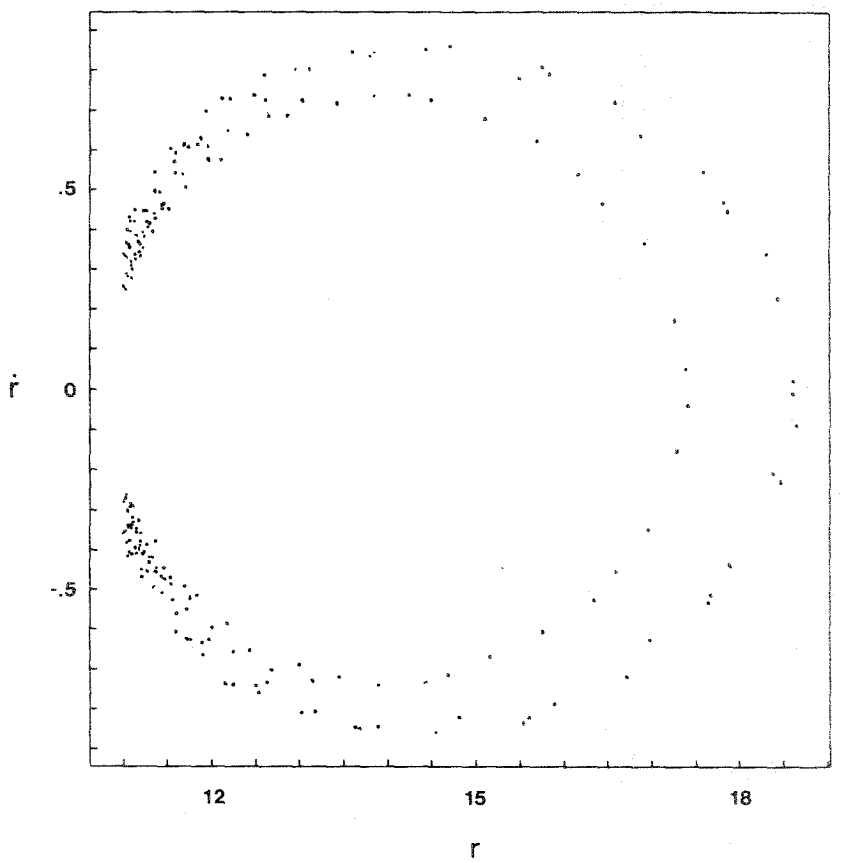

FIG. 10. Another surface of section plot for the particle of Fig. 8, but with diagnostics performed every timestep. Less spread in the pattern is evident.

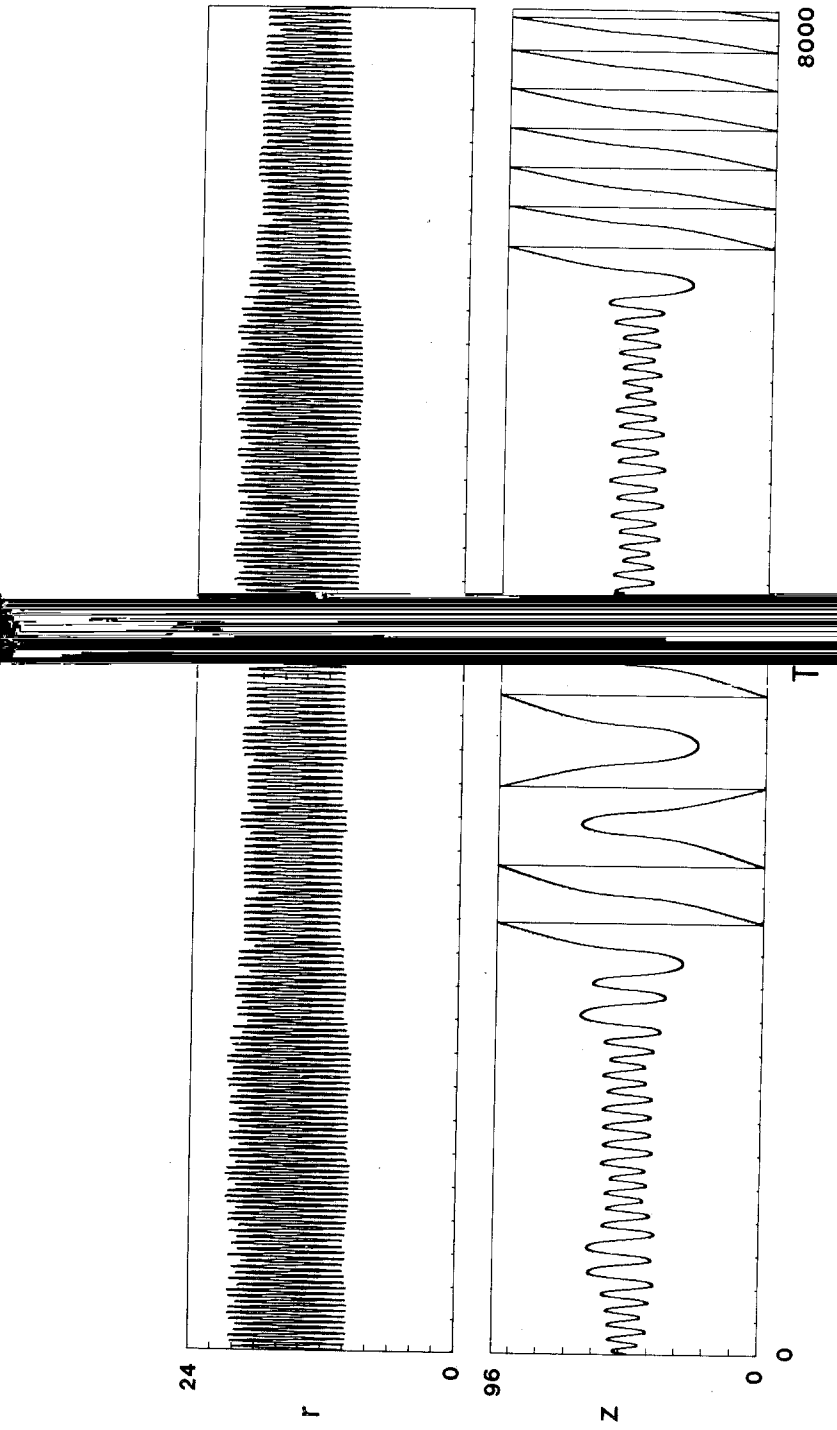

FIG. 11. R and z histories for a stochastic particle from the same run.

trajectory moves. If the particle orbit is to sweep out a nonzero volume of this space, it must also sweep out a nonzero area of the slice. To make the plots, a postprocessor program was written. It extracted the tracer particle histories of r and z as functions of time from a printed output file, which was generated by RINGHYBRID and rearranged using a text editor. The program computed the instants of time at which $z = L/2$ was crossed using linear interpolation on the history of z. Again using linear interpolation, the values of r at these same instants were calculated from the r history. Finally, the associated values of $\dot{r}$ were calculated by a simple finite difference. While this interpolation scheme is of low order, it appears to be reasonably effective when small timesteps are taken and the histories are arranged so as to save every point of the trajectory. Furthermore, it can be argued that the simple leapfrog mover used by the codes does not justify a higher-order interpolation scheme, though this point is not entirely clear.

Illustrated in Fig. 8 are the r and z histories of a nonstochastic particle selected

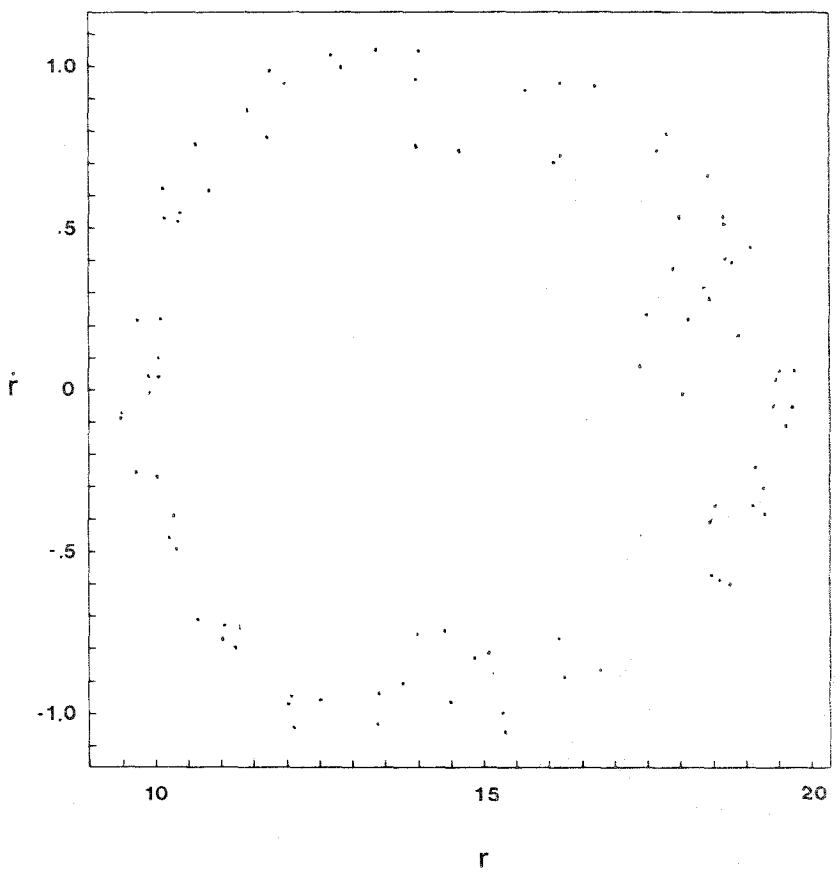

FIG. 12. Surface of section plot for the stochastic particle of Fig. 11. The points fill an annular region, and are not confined to the outline of a region as was the case for the particle of Figs. 8–10.

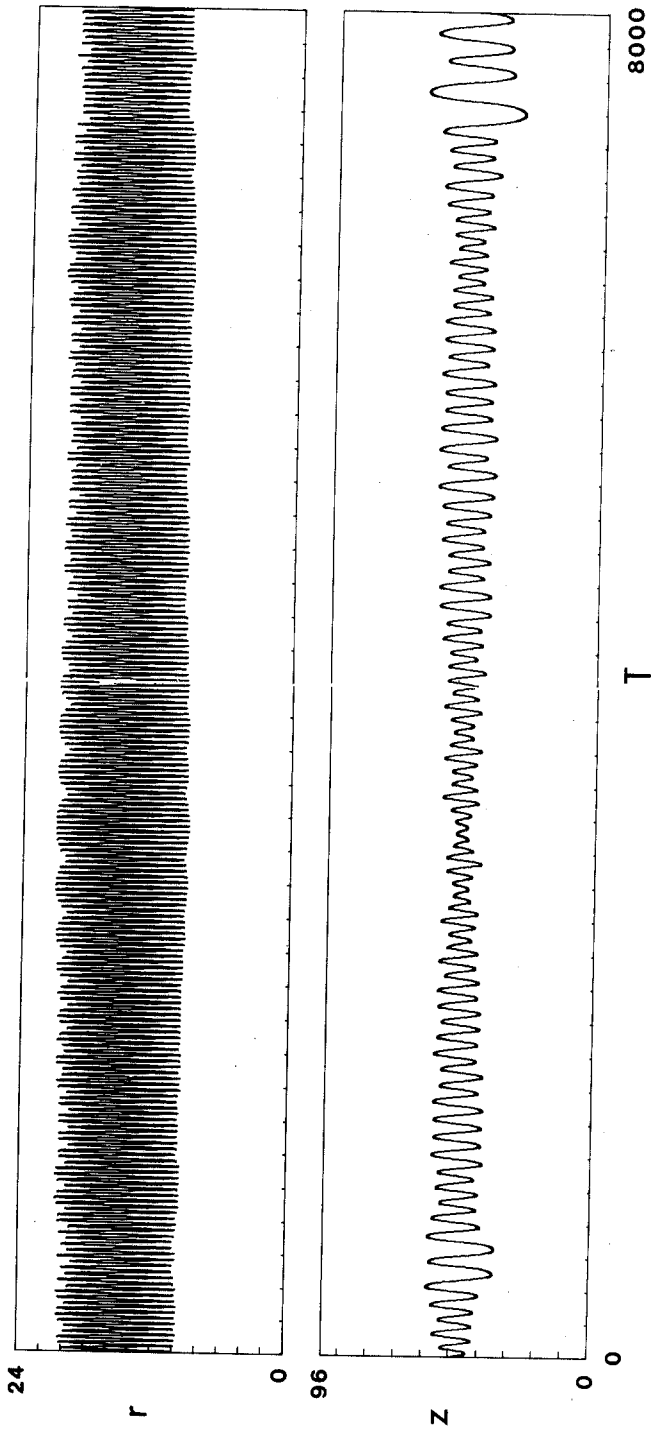

FIG. 13. R and z histories for the particle that was initially the mirror image of the particle of Figs. 11 and 12. This particle appears to be confined—in fact it becomes unconfined at timestep 8400, beyond the end of this plot.

from a run with $L = 96$. The plot shows the trajectory over 8000 timesteps, a very long run for the code. In Fig. 9 the surface of section plot for this particle is shown. Fields were "frozen" at timestep 450 and every other timestep was saved in the history file; the plot shows points taken from the interval between timesteps 452 and 8000. The plane $z = L/2$ was crossed 235 times during this time. Points in this plot are observed to fall on a crescent-shaped curve, without filling in the area of the crescent. There is, however, considerable raggedness to the plot, which may be ascribed to the finite timestep and the diagnostic interval of two. The raggedness is an artifact of the algorithm used to generate the plot, and does not result from orbital stochasticity. To demonstrate this, Fig. 10 shows a surface of section for the same particle using a diagnostic interval of one step and starting from timestep 451. The curve is seen to be much smoother than that of Fig. 9. This example illustrates the need for care in the implementation of such diagnostics, to prevent false indications of stochasticity.

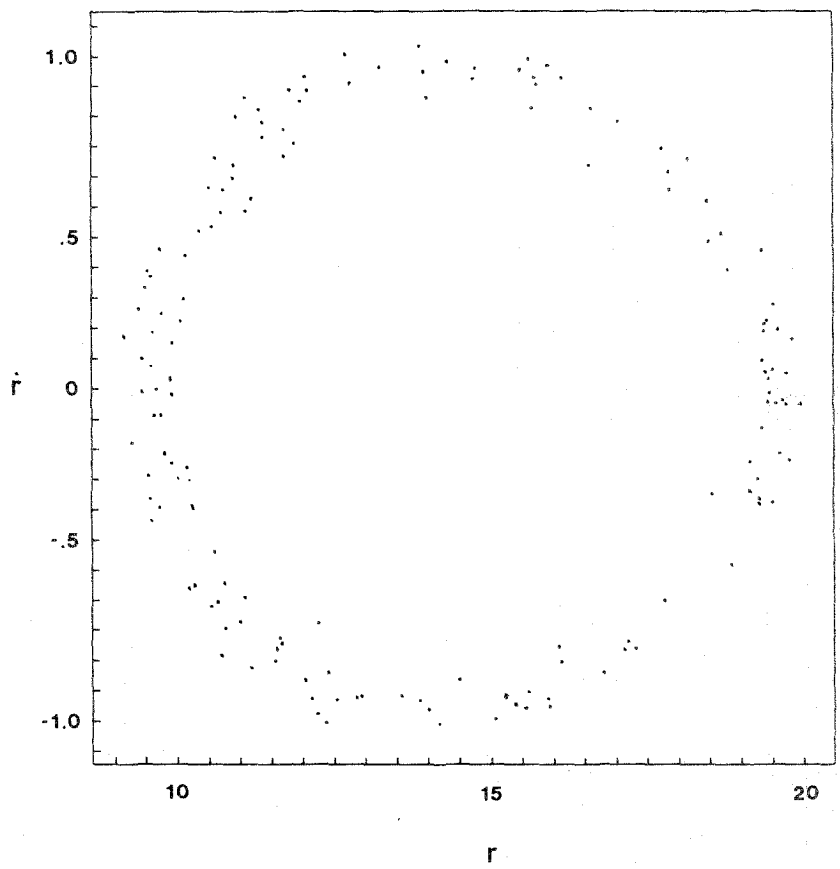

FIG. 14. Surface of section plot for the particle of Fig. 13.

The orbit of a stochastic particle from the same run is shown in Fig. 11. The particle is not bound and the periodicity condition is enforced a number of times, the first time being approximately at timestep 2600. The surface of section plot for this particle is shown in Fig. 12. Diagnostics were made every timestep. For this trajectory there were 89 crossings of $z = L/2$. There is evidently a qualitative difference between this orbit and the previous one, as here the points do not lie on a smooth curve but appear to fill an annular region of the plane. The orbit of the particle that was initialized to be the mirror image of the particle in Fig. 11 is shown in Fig. 13. In contrast with its "mirror image," this particle appears to be bound for the 8000 timesteps illustrated. In fact, a continuation of the run shows this particle to be unbound, first reaching the end of the system at timestep 8400. It would be surprising were this not the case, as the same regions of phase space should normally be acessible to both of a mirror image pair of stochastic particles. The surface of section plot for this trajectory is shown in Fig. 14; in fact, this plot and that of Fig. 12 might be superposed to give a clearer picture of the area of the $r - \dot{r}$ plane accessible. There were 154 crossings of $z = L/2$ in this case.

IV. Stochasticity in the Linearized Simulation

A. *Observation*

The second manifestation of the diverging trajectories is of much greater fundamental concern. In the first order linearization, we consider the motion of a "displaced point" P' relative to that of an unperturbed point P [10]. The vector separation between the two is denoted as $\boldsymbol{\varepsilon}$. Point P' also moves in the zero order field, but this field is evaluated at the perturbed location, while the field for particle P is evaluated at the unperturbed location. Since the points P and P' represent neighboring trajectories, when orbits are stochastic we can expect the magnitude of $\boldsymbol{\varepsilon}$ to increase exponentially with time whether or not Eulerian first-order fields are included in the calculation, since the stochastic separation is due to particle motion in the inhomogeneous zero order field. This is in fact the observed behavior.

Figure 15 shows part of a non-stochastic particle orbit (r and z versus time) selected from a run with the parameters of KBA. This is the same particle plotted in Fig. 8; timesteps 2000 to 4000 are shown here in detail. For this particle, time histories of the magnitudes of the r, θ, and z components of $\boldsymbol{\varepsilon}$ are plotted in Fig. 16. The initial excitation was implemented by giving all particles a positive first order axial velocity $\dot{\varepsilon}$ at timestep 500, and no Eulerian first order fields were included in the calculation. All components of $\boldsymbol{\varepsilon}$ are seen to oscillate steadily. This may be contrasted with the behavior of the stochastic particle of Fig. 11, part of the orbit of which is shown in greater detail in Fig. 17. As seen in Fig. 18, all components of $\boldsymbol{\varepsilon}$ grow noisily. Figure 19 shows the time histories of the components of the mean $\boldsymbol{\varepsilon}$ obtained by averaging over all particles. The mean ε_z shows stable oscillation at first, as would be expected without any first order field response to drive kink modes, etc., but soon

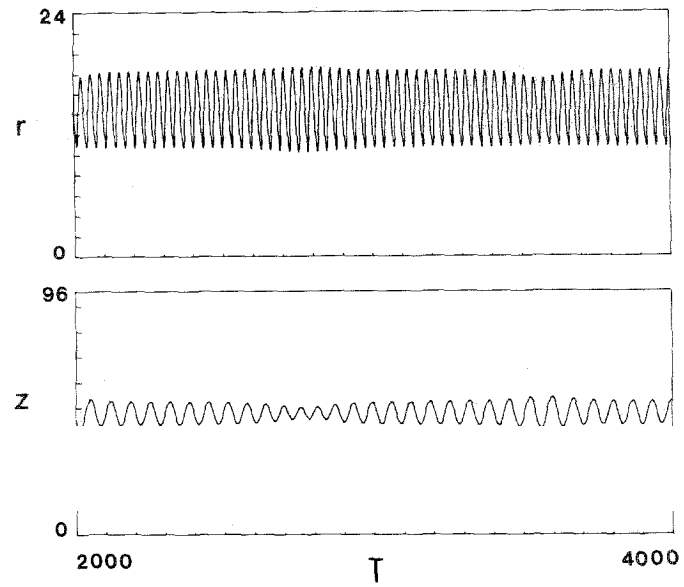

FIG. 15. Expanded r and z histories for the nonstochastic particle of Figs. 8–10.

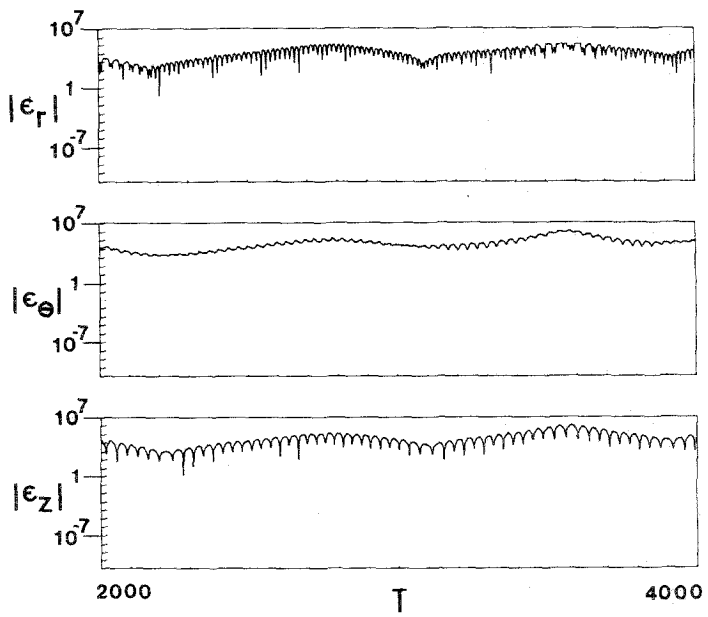

FIG. 16. Time histories of the magnitudes of the r, θ, and z components of $\boldsymbol{\varepsilon}$ for the nonstochastic particle of Figs. 8–10 and 15.

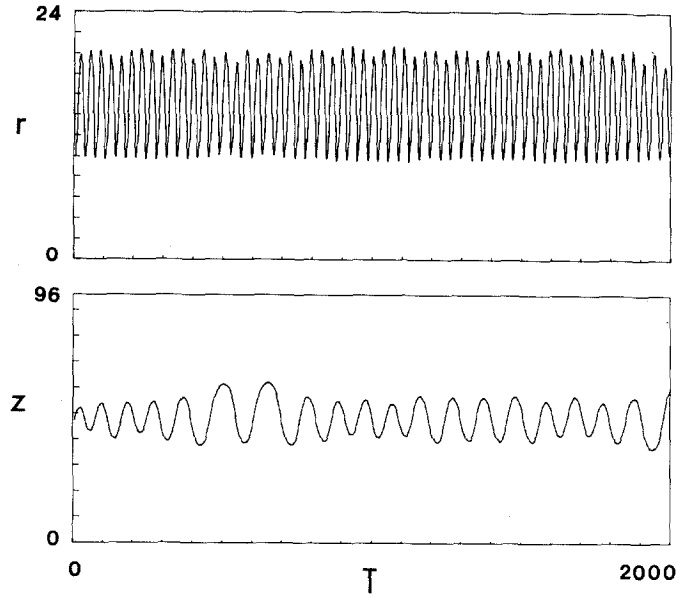

FIG. 17. Expanded r and z histories for the stochastic particle of Figs. 11 and 12.

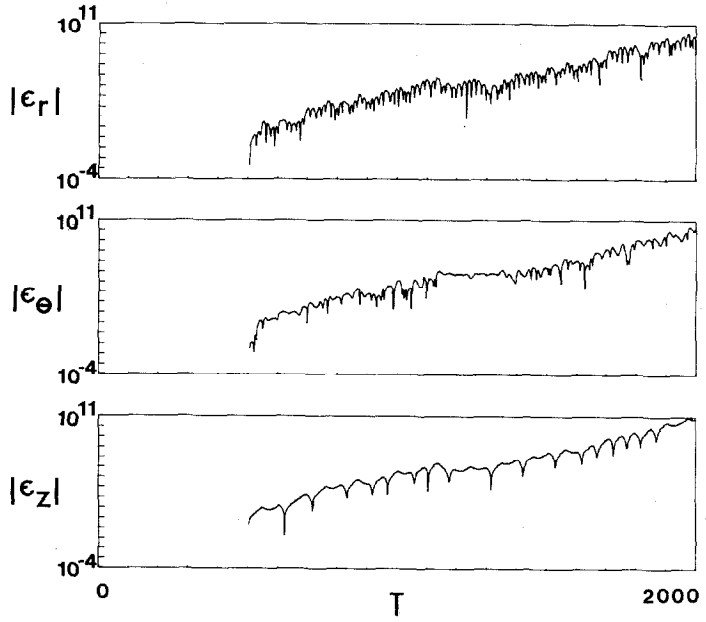

FIG. 18. Time histories of the magnitudes of the r, θ, and z components of ε for the stochastic particle of Figs. 11, 12, and 17. Noisy growth is evident.

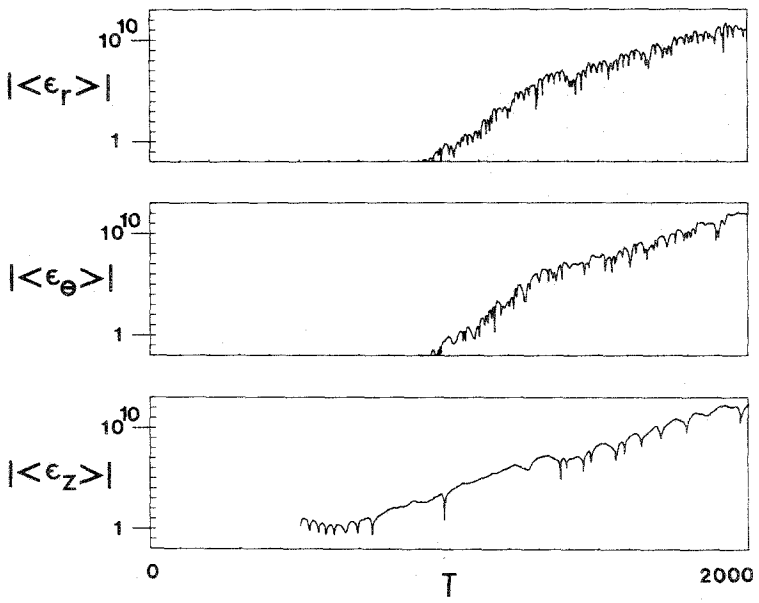

FIG. 19. Time histories of the magnitudes of the mean r, θ, and z components of ε obtained by averaging over all particles.

the ragged growth characterizing the single-particle modes takes over. The r and θ mean components are initially zero due to the symmetry of the first order initialization. As symmetry breaks down they grow rapidly to a level comparable to that of the z components, then grow at the same (slower) rate as the latter. This is because the three components of $\boldsymbol{\varepsilon}$ are mutually coupled for each particle, as seen in the previous figure. The growth is even faster in runs with a shorter periodicity length L.

When the term $\mathbf{v}_0 \times (\boldsymbol{\varepsilon} \cdot \nabla)\, \mathbf{B}_0$ in the linearized equation of motion is deleted, the first order motion is observed to become stable. To understand this lack of growth note that, by taking the scalar product of $(\mathbf{v}_0 + \dot{\boldsymbol{\varepsilon}})$ with the linearized equation of motion for the same quantity,

$$d/dt[(\mathbf{v}_0 + \dot{\boldsymbol{\varepsilon}})^2] = 2\dot{\boldsymbol{\varepsilon}} \cdot [\mathbf{v}_0 \times (\boldsymbol{\varepsilon} \cdot \nabla)\, \mathbf{B}_0],$$

so that $\dot{\boldsymbol{\varepsilon}}$ cannot grow indefinitely when the right-hand side is zero. This term is responsible for making the orbit of P' a neighboring orbit to that of P, and not an identical orbit as when the term is omitted.

Because of the relationship between high energy (large excursion) and stochasticity, an attempt was made to eliminate the large-excursion particles by placing "sticky" walls at $Z = 6$ and 18, in a run with $L = 24$. While 400 of the 2400 particles were removed, stochastic growth of $\boldsymbol{\varepsilon}$ was still present, and the maximum growth rate was only slightly less than in the comparable run made without the sticky walls. See also the discussion of run KKA in Section III.B above.

B. *Implications*

This type of dynamical instability is quite distinct from the collective plasma effects we wish to examine. In a true Vlasov plasma with an infinite number of particles, the random phases of the growing displacements ε for all particles would be expected to cancel out in the mean, and no gross plasma moments would be affected. However, in a simulation plasma with perhaps one to ten thousand particles, this may not be the case. Since different particles have different growth rates, the single-particle growth of one or a few particles comes to dominate, and when we examine moments such as mean ε, first order currents, etc. the only thing that appears is the effect of this one or few particles. Unless the collective modes have a higher growth rate than the fastest growing single particle mode, only the latter can be seen, and regardless of background plasma parameters the growth will appear the same.

If one attempts to minimize the stochastic growth by increasing the number of particles, the reduction is small since the cancellation should improve only as the square root of the number of particles. Attempts to reduce the mean rate of growth by employing up to 9600 particles were unsuccessful, possibly because when more particles were used some fell on orbits with even higher associated growth rates. Cancellation would possibly occur if a far greater number of particles were employed, but no clear dependence of the stochastic growth rate upon the number of simulation particles has been observed.

J. M. Finn has observed, in computer experiments using model potentials, a strong model dependence of the stochastic properties [1]. In two of three models, including one self-consistent model, he observes predominantly stochastic behavior, while in the last (nonself-consistent) model he observes only limited stochastic behavior. Larrabee and Lovelace, using a different self-consistent model developed for studies of ion ring compression, find stochastic orbits to be present only in the minority of cases [3]. They suggest that meaningful conclusions about the stochasticity of orbits can be drawn by examination of the parameters describing the bottom of the effective potential well, and the stability of orbits which exhibit little excursion in the axial direction. A class of field reversed ring equilibria which excludes stochastic motion because the spatial dependence of A_θ is such that other constants of the particle motion are explicitly present has been described by Channell [4]. These equilibria also have the property that all particles are confined. However, to data no actual examples have been constructed. By suitable choice of model it is thus possible to find equilibria with only weak single-particle growth, or none at all. This necessarily entails a serious restriction on the class of problems which can be run.

Discrete representations of numerically calculated Vlasov equilibria afford complete control over the particle distribution, while equilibria formed by injection, as described herein, are rather likely to encompass stochastic orbits. However, recent work employing exponential rigid rotor equilibria computed on a grid has shown that these equilibria entail a significant fraction of stochastic orbits also [12, 13], and thus equilibria other than the exponential rigid rotor may be more tractable for linearized simulation. Furthermore, even some equilibria formed by injection are

usable; in one fully field reversed ring with an aspect ratio of order 4 : 1 the stochastic growth is slow enough that meaningful conclusions about collective behavior can be drawn from the results. Studies of ion ring stability employing this equilibrium will be described in a later paper [23].

It may be possible to treat problems involving stochastic orbits by other means. Perhaps the fastest-growing particles can be removed from the computation artificially, at some risk of affecting the physics. This may be most reasonable for mirror plasmas where only a small fraction of the particles are both axis-encircling and stochastic. To date we have had little success with this approach. A more

distribution function f in a moment conserving manner, as a means of smoothing out the single-particle effects. We have had some preliminary success with a reconstruction technique that assumes a "rigid" perturbation, i.e., one for which the mean displacement of particles in the poloidal plane is approximately independent of position in that plane [13, 23]. To see how this works, refer to Fig. 19, and note that a smooth coherent behavior (a damped, phase-mixing oscillation) dominates the mean axial displacement for a period of time before the single-particle instability has had a chance to exponentiate from the very low level associated with roundoff and/or asymmetry to a large level. By periodically setting the displacement of each particle equal to the mean displacement of all particles (and similarly for the first order velocities), the coherent perturbation of a rigid mode is preserved, while the random part is reset to zero before it can dominate. Using this technique, we have been able to observe both unstable and stable tilting motions of an exponential rigid rotor ion ring [23]. Even though the true mode may not be perfectly rigid, its projection onto a rigid displacement is often large enough for the technique to work.

We believe that a more general "local" reconstruction algorithm is possible, at least for fluidlike modes for which the dominant perturbation in the displacement field at each point in space is single valued. The first order displacement and velocity of each particle might be set equal to the averages of these quantities over all particles in the cell, or an area-weighting procedure might be used [25]. Alternately, local or global fieldline averages might be used for flute or balooning modes, yielding better statistics at the expense of generality in the mode structure. Orbit averaging might be used to improve the particle statistics, since the modes of interest are generally of low frequency, while the noise in large part is of higher frequencies.

The most general reconstruction would involve averaging the displacement of a particle only with the displacements of the particle's neighbors in phase space; in principle, such a scheme could be employed in the study of modes having arbitrary structure.

V. Conclusions

In summary, the effects of stochastic single-particle orbits have been observed in a series of computer simulations of strong ion rings. It is anticipated that they are also

present in a wide class of systems such as field-reversed mirror plasmas with large nominal gyroradii. Nonlinear axisymmetric codes are able to treat problems involving stochastic orbits with only minor difficulties. These include an eventual violation of mirror symmetry and small fluctuations in a normally conserved momentum. Linearized codes, however, are more severely affected by the presence of stochastic orbits. The exponential growth of the displacement between unperturbed and perturbed trajectories can be sufficiently rapid as to mask the collective modes which are the true objects of study. Fully nonlinear 3d codes may also experience difficulties when stochastic orbits are present, if the intuitively noise-reducing "quiet-start" technique of loading particles on axisymmetric rings (in the present geometry) or straight rods, etc. (in other geometries) is employed. The linear growth phase of instabilities may be masked as it is in the linearized simulations, and modes might even saturate at lower levels than the level associated with cessation of exponential orbit separation. If no "quiet" loading is employed, a very large number of particles is likely to be needed to see linear growth, since small excitations will normally be invisible due to the high fluctuation level associated with the discreteness of the distribution.

By careful choice of equilibria, straightforward linearized simulation can still be a useful tool for the study of Vlasov stability. When suitable "reconstruction" algorithms have been developed and implemented, this type of simulation should be applicable to a wider class of problems.

ACKNOWLEDGMENTS

The authors wish to acknowledge useful discussion with C. K. Birdsall, J. A. Byers, R. H. Cohen, J. M. Finn, M. J. Gerver, and E. C. Morse. The support afforded by Prof. Birdsall is appreciated.
This work was supported by the U. S. Department of Energy.

REFERENCES

1. J. M. FINN, *Plasma Phys.* **21** (1979), 405.
2. R. H. COHEN, Stochastic Motion of Particles in Mirror Machines, *in* "Intrinsic Stochasticity in Plasmas" (G. Laval and D. Gresillon, Eds.), Editions de Physique, Orsay, 1979; and private communication.
3. D. A. LARRABEE AND R. V. LOVELACE, *Phys. Fluids* **23** (1980), 1436.
4. P. J. CHANNELL, *Phys. Fluids* **23** (1980), 1263.
5. B. V. CHIRIKOV, *Phys. Rep.* **52** (1979), 263.
6. G. BENETTIN, L. GALGANI, AND J.-M. STRELCYN, *Phys. Rev. A* **14** (1976), 2338.
7. J. M. GREENE, *J. Math. Phys.* **20** (1979), 1183.
8. V. I. ARNOLD AND A. AVEZ, "Ergodic Problems of Classical Mechanics," New York, Benjamin, 1968.
9. R. H. BERMAN, *Bull. Amer. Phys. Soc.* **24** (1979), 942.
10. A. FRIEDMAN, R. N. SUDAN, AND J. DENAVIT, *J. Comp. Phys.* **40** (1981), 1; see also paper number PC-13, Proc. Eighth Conf. on Numerical Simulation of Plasmas, Monterey, CA, June 28–30 (1978).

11. D. O. DICKMAN, R. L. MORSE, AND C. W. NIELSON, *Phys. Fluids* **12** (1969), 1708.
12. A. FRIEDMAN, "FRM and Ion Ring Equilibria for the RINGHYBRID Code," Proc. 1980 Sherwood Theory Meeting, Tucson, Arizona (1980).
13. A. FRIEDMAN, "Field Reversed Equilibria, Intrinsic Stochasticity, and Collective Stability," Proc. Ninth Conf. on Numerical Simulation of Plasmas, Paper No. OB-3, Evanston, Illinois (1980).
14. N. C. CHRISTOFILOS, *Plasma Physics and Controlled Nuclear Fusion* 1 (1959), 576.
15. M. BRETTSCHNEIDER, J. KILLEEN, AND A. A. MIRIN, *J. Comp. Phys.* **11** (1973), 360.
16. J. A. BYERS, J. P. HOLDREN, J. KILLEEN, A. B. LANGDON, A. A. MIRIN, M. E. RENSINK, AND C. G. TULL, *Phys. Fluids* **17** (1974), 2061.
17. A. FRIEDMAN, R. L. FERCH, R. N. SUDAN, AND A. T. DROBOT, *Plasma Phys.* **19** (1977), 1101.
18. A. MANKOFSKY, A. FRIEDMAN, AND R. N. SUDAN, *Plasma Phys.* **23** (1981), 521.
19. R. V. LOVELACE, *Phys. Fluids* **19** (1976), 723.
20. R. V. LOVELACE, D. A. LARRABEE, AND H. H. FLEISCHMANN, *Phys. Fluids* **21** (1978), 863.
21. R. V. LOVELACE, D. A. LARRABEE, AND H. H. FLEISCHMANN, *Phys. Fluids* **22** (1979), 701.
22. G. SCHMIDT, "Physics of High Temperature Plasmas," pp. 29–44, Academic Press, New York, 1966.
23. A. FRIEDMAN, *Bull. Amer. Phys. Soc.* **25** (1980), 970.
24. R. H. G. HELLEMAN, Self-Generated Chaotic Behavior in Nonlinear Mechanics, *in* "Fundamental Problems in Statistical Mechanics," Vol. 5 (E. G. D. Cohen, Ed.), pp. 165–233, North-Holland, Amsterdam/New York, 1980.
25. A. FRIEDMAN, Proc. Ninth Conf. on Numerical Simulation of Plasmas, Evanston, Ill., 1980.